Atomic-Scale Issues in Tribology: Interfacial Junctions and Nano-elastohydrodynamics[†]

Uzi Landman,* W. D. Luedtke, and Jianping Gao

School of Physics, Georgia Institute of Technology, Atlanta, Georgia 30332

Received October 17, 1995. In Final Form: March 6, 1996[⊗]

Advances in computer-based modeling and simulation methodologies and capabilities, coupled with the emergence and development of high-resolution experimental techniques, allow investigations of tribological phenomena with unprecedented atomic-scale spatial and temporal resolution. We focus here on molecular dynamics simulations of formation and properties of interfacial junctions and on nano-elastohydrodynamics in sheared lubricated junctions. Simulations predict that upon approach of a metal tip to a surface a jump-to-contact instability occurs and that subsequent nanoindetation leads to plastic deformation of the gold surface. Retraction of the tip from the surface results in formation of a connective junction, or wire, of nanoscale dimensions, whose elongation mechanism consists of a series of plastic stress-accumulation and stress-relief stages which are accompanied by structural order−disorder transformations. These transformations involve multiple-glide processes. The yield-stress of a gold nanowire is predicted to be ∼3 GPa, which is an order of magnitude larger than that of bulk gold. Comparisons of the structural, mechanical and electrical properties of nanowires generated via elongation of junctions of initial very different dimensions, confirms that nanowires of similar nature are formed, irrespective of the history of the junctions. Shearing the junction occurs via an atomic-scale stick−slip mechanism characterized by a similar critical stress. The elongation process is reflected in hysteresis in the force versus tip-to-surface distance records, and in oscillatory behavior of the force. Measurements of room-temperature electronic transport in such pulled gold nanowires reveal periodic conductance quantization steps, in units of $2e^2/h$. Simulations of atomic-scale structure, dynamics, flow, and response characteristics of a thin film molecular hexadecane lubricant, confined and sheared by topographically nonuniform solid gold surfaces sliding at a relative velocity of 10 m/s, are described. The simulations reveal nanoscale processes which include the following: spatial and temporal variations in the density and pressure of the lubricant, particularly in the region confined by the approaching asperities, accompanied by asperity-induced molecular layering transitions which are reflected in oscillatory patterns in the friction force; dynamical formation of elastoplastic, or glassy, states of the lubricant in the interasperity zone; drastic asperity deformations mediated by the lubricant, leading to microstructural transformations of the nonuniform bounding solid surfaces; molecular trapping and formation of intermetallic junctions; and onset of cavitated zones in the lubricating fluid after the asperity−asperity collision process. The simulations extend micro-elastohydrodynamic continuum investigations into the nanoscale regime and provide molecular-scale insights into the fundamental mechanisms of ultrathin film lubrication phenomena under extreme conditions, which are of significance for modern technologies.

1. Introduction

Tribological phenomena, including friction, wear, and lubrication, occur whenever two material bodies are brought together and translated with respect to each other. The goals of explorations of these phenomena, dating back to antiquity,[1] are to understand their physical and chemical origins and to design ways and means for minimizing losses (energy dissipation, materials degradation, and wasted materials and human resources) related to such processes.

Tribological phenomena occur in systems encompassing a broad spectrum of scales (spatial and temporal), from common machine, instrument, and tool elements (such as a ball bearing and its race groove, a pair of spur gear involute teeth, cams and shafts, and the components of polishing, machining, and patterning instruments), to high-density data storage devices (e.g., read/write heads and recording media at nanoscale promixity), micromachines, and biotribological systems[2] (such as synovial joints and total joint replacements). Common to all the aforementioned systems is their interfacial junction configu-

ration and, in case of lubricated junctions, the confined environment of the lubricating fluid between the interfacing solid surfaces. Consequently, studies of the basic origins of tribological phenomena focus on investigations of the formation mechanisms and properties of interfacial solid and liquid junctions, interfacial adhesion, and the structure, dynamics, flow, and rheology of complex liquids under confinement and during shear. Such observations date back many years; indeed a forerunner to the Bowden and Tabor[3] description of friction as the force to shear interfacial junctions (formed when surfaces touch at the tips of their asperities which readily undergo plastic deformation so that each asperity makes contact over an area proportional to the load it bears), plus the force required to plow the surface of the softer surface by the asperities of the harder one, is the observation made by Desaguliers[4] in 1734 in the context of studies of surface finish that "... the flat surfaces of metals or other Bodies may be so far polished as to increase Friction and this is a mechanical Paradox: but the reason will appear when we consider that the Attraction of Cohesion becomes sensible as we bring the Surfaces of Bodies nearer and nearer to Contact." Furthermore, the current views that the general purposes of a lubricating fluid are to provide protective coating to the solid surfaces thus preventing

[†] Presented at the Workshop on Physical and Chemical Mechanisms in Tribology, held at Bar Harbor, ME, August 27 to September 1, 1995.

[⊗] Abstract published in *Advance ACS Abstracts,* Sept. 15, 1996.

(1) Dowson, D. *History of Tribology*; Longman: New York, 1979.

(2) *An Introduction to the Bio-Mechanics of Joints and Joint Replacements*, Dowson, D., Wright, V., Eds.; Mechanical Engineering Publications: Bury St. Edmunds, 1978; see also ref 11, p 485.

(3) Bowden, F. P.; Tabor, D. *Friction*; Anchor Press/Doubleday: Garden City, NY, 1973; *The Friction and Lubrication of Solids*, Parts I and II; Clarendon: Oxford, 1950 and 1964.

(4) Desaguliers, J. T. *A Course of Experimental Philosphy*, 2 Vols; London, 1734; Vol. I, with thirty-two copper plates.

formation of an adhesive junction and to reduce frictional losses by acting as an interfacial layer of low shear strength, and even the more recent development[5-7] in the 1960s of the theory of elastohydrodynamic lubrication (EHL), may find their origins in early observations, such as "some people put on the ground planed boards because of their smoothness and smear them with grease, because the roughness that is on them is made smooth and so they move the burdens with smaller power" (Heron of Alexandria (ca. 60 A.D.)), and those made by John Leslie in 1804 concerning the deformation loss aspect of friction, where he writes[8] "... The intervention of a coat of oil, soap or tallow, by readily accommodating itself to the variations of contact, must tend to equalize it, and therefore must lessen the angles, or soften the contour, of the successively emerging prominences, and thus diminish likewise the friction which thence results. Such is apparently the real origin or friction."

Understanding the atomistic mechanisms, energetics, structure, and dynamics underlying tribological processes is fundamentally important to many basic and applied problems (such as adhesion, capillarity, wetting, contact formation, interfacial junctions, surface deformation, hardness, micro- and nanoindentation, states and rheology of confined complex liquids, thin film lubrication, wear, fracture, atomic-scale probing, and modifications and manipulations of materials surfaces). Explorations of materials systems and phenomena in the nanoscale regime often require experimental probes and theoretical and computational methods that allow investigations with refined spatial, as well as temporal, resolution. Consequently, until recently most theoretical approaches to the above issues, with a few exceptions, have been anchored in continuum elasticity and contact mechanics.[9-13] Experimental observations and measurements of surface forces and the consequent materials response to such interactions have been macroscopic in nature.

The quest to observe and understand natural phenomena on refined microscopic scales and the ever increasing trend toward device miniturization has led to the development of conceptual and technological devices that allow the interrogation of materials with increasing resolution. Such endeavors, enabled by the advent and proliferation of microscopies and local probes with atomic-scale spatial resolution[14,15] (particularly tip-based microscopies such as scanning tunneling (STM) and atomic force (AFM) microscopies and the surface force apparatus (SFA)), in conjunction with improved understanding of the nature of cohesion and bonding in materials, formulation and implementation of new computational techniques and computer-based simulation methods, and the introduction of new computer technologies and computational strategies (e.g., vector and more recently parallel computers), open new avenues of investigations of the microscopic origins of materials phenomena in general, interfacial processes in particular, and direct confrontation of experimental observations with theoretical predictions.[16,17]

In this article, we focus, by way of examples, on computer simulations, where the evolution of a physical system is simulated, with refined temporal and spatial resolution, via a direct numerical solution of the equations of motion (quantum or classical). These methods alleviate certain of the major difficulties that hamper other theoretical approaches, particularly for complex systems such as those characterized by a large number of degrees of freedom, lack of symmetry, nonlinearities, and complicated interactions. Furthermore, using these methods allows theorists to help explain and elucidate results of specific experiments, guide the developments of concepts, principles, and theories unifying a range of observations, and predict new behavior.

To illustrate computer simulation methods and the deep insights gained through such studies we focus on two main topics: (i) formation and properties of interfacial solid and liquid junctions, and (ii) nanoelastohydrodynamics in sheared lubricated junctions.

Some of the results obtained via such atomistic simulations[16-19] correlate with the predictions of theories constructed on the basis of macroscopic considerations, thus providing a microscopic foundation for rigorous derivations of such descriptions and allow assessment of their range of validity and applicability. On the other hand it was also found that molecular structure, thermodynamics, mechanical response, rheology, and molecular dynamics at interfaces and in confined thin films are often very different from that in the bulk and cannot be understood by simple extrapolation of bulk properties. Such findings include atomic-scale adhesion and interfacial wetting phenomena occurring upon contact formation,[16b,17,18] generation of atomic-scale connective junctions occurring upon approach and separation of small intermetallic (as well as ionic or covalently-bonded) contacts,[17-19] atomic-scale stick—slip friction occurring upon sliding,[20] the ability of confined molecularly thin liquid films to support high normal loads,[21] and structural ordering and phase transitions of dynamic nature occurring in thin lubricant films pressed and sheared between confining solid boundaries.[21-28] Investigations of these phenomena, which occur on characteristic atomic and

(5) Dowson, D.; Higginson, G. R. *Elastohydrodynamic Lubrication*; Pergamon: London, 1977.

(6) Gohar, R. *Elastohydrodynamics*; Horwood: Chichester, 1988.

(7) Dowson, D. In *Fundamentals of Friction: Macroscopic and Microscopic Processes*, Singer, I. L., Pollock, H. M., Eds.; Kluwer: Dordrecht, 1992; p 325.

(8) Leslie, J. *An Experimental Inquiry Into the Nature and Progation of Heat*, printed for Newman, J.; No. 22, Poultry, England, 1804.

(9) Hertz, H.; Reine, *J. Angew. Math.* **1882**, *92*, 156; also in *Miscellaneous Papers*; Macmillan: London, 1896; p 146; see review by Johnson, K. K. *Pro. Instrm. Mech. Eng.* **1982**, *196*, 363.

(10) Johnson, K. L. *Contact Mechanics*; Cambridge University Press: Cambridge, 1985.

(11) Johnson, K. L.; Kendall, K.; Roberts, A. D. *Proc. R. Soc. London, Ser. A* **1971**, *324*, 301.

(12) Derjaguin, B. V.; Muller, V. M.; Toporov, Yu. P. J. *Colloid Interface Sci.* **1975**, *53*, 314. Muller, V. M.; Derjaguin, B. V.; Toporov, Yu. P. *Colloids Surf.* **1983**, *7*, 251.

(13) Israelachvili, J. N. *Intermolecular and Surface Forces*, 2nd ed.; Academic Press: New York, 1992.

(14) (a) See articles in ref 7. (b) For a recent review see: Bhushan, B., Israelachvili, J. N.; Landman, U. *Nature* **1995**, *374*, 607.

(15) *Handbook of Micro/Nano Tribology*; Bhushan, B., Ed.; CRC Press: Boca Raton, FL, 1995.

(16) (a) Landman, U.; Barnett, R. N.; Cheng, H.-P.; Cleveland, C. L.; Luedtke, W. D. In *Computations for the Nano-Scale*; Bloch, P. E., Joachim, C., Fisher, A. J., Eds.; Kluwer: Dordrecht, 1993; p 75. (b) See also Landman, U.; Luedtke, W. D.; Ringer, E. M. In ref 7, p 463.

(17) Landman, U.; Luedtke, W. D.; Burnham, N. A.; Colton, R. J. *Science* **1990**, *248*, 454.

(18) Luedtke, W. D.; Landman, U. *Comput. Mater. Sci.* **1992**, *1*, 1.

(19) Landman, U.; Luedtke, W. D. *J. Vac. Sci. Technol., B* **1991**, *9*, 414.

(20) (a) Landman, U.; Luedtke, W. D.; Nitzan, A. *Surf. Sci.* **1989**, *210*, L177. (b) Landman, U.; Luedtke, W. D.; Ribarsky, M. W. *J. Vac. Sci. Technol.* **1989**, *A7*, 2829.

(21) Ribarsky, M. W.; Landman, U. *J. Chem. Phys.* **1992**, *97*, 1937.

(22) Rhykerd, C. L.; Choen, M. S.; Diester, D.; Cushman, J. *Nature* **1987**, *380*, 461. Schoen, M.; Rhykerd, C. L.; Diesther, D. J.; Cushman, J. H. *Science* **1989**, *245*, 1223. Diester, D.; Schoen, M.; Cushman, J. *Science* **1993**, *262*, 545.

(23) Thompson, P. A.; Robbins, M. O. *Science* **1990**, *250*, 792.

(24) Robbins, M. O.; Thompson, P. A. *Science* **1991**, *253*, 916.

(25) Thompson, P. A.; Grest, G. S.; Robbins, M. O. *Phys. Rev. Lett.* **1992**, *68*, 3448.

(26) Persson, B. N. J. *Phys. Rev. B* **1994**, *50*, 4771.

(27) Gupta, S.; Koopman, D. C.; Westerman-Clark, G. B.; Bitsanis, I. A. *J. Chem. Phys.* **1994**, *100*, 8444.

(28) Wang, Y.; Hill, K.; Harris, J. G. *J. Chem. Phys.* **1994**, *100*, 3276.

molecular spatial and temporal scales, are outside the domain of continuum treatments, requiring instead the application of experimental and theoretical methodologies with refined atomic-scale resolution.

2. Solid and Liquid Junctions

To address issues pertaining to the formation and properties of solid and liquid junctions, we have embarked on a series of investigations of the energetics, mechanisms, and consequences of interactions between material tips and substrate surfaces (ionic, covalent, and metallic), with and without intervening adsorbed organic films.[16-20,29,30] In these large scale simulations the solid surfaces were described by appropriate interatomic interactions (in particular, for metals we have employed embedded atom potentials[16b,17]); intra- and intermolecular interactions in the model lubricant *n*-alkane films were modeled through united-atom interaction potentials,[31,32] which include bond-stretch, bond-bending, dihedral-angle, and nonbonded interactions, and the interactions between the molecular segments and the substrate atoms were described via potentials fitted to experimentally measured adsorption energies.[21,32]

(a) Solid Junctions. Solid junctions are materials structures which form upon bringing bodies into proximal interaction, during the separation of contacting bodies, or in the process of extension (e.g., pulling) of a material system. Past, as well as intensifying current, investigations of junctions have been motivated by the ubiquity of circumstances in which they may be formed, either naturally in the course of a physical process (as in the case of materials interfaces in relative motion with respect to each other where the frictional resistance to shear has been attributed[3,14,17] to the formation of interfacial junctions, or as the source of interfacial adhesive action), or intentionally (e.g., controlled generation of wires via the extension of materials contacts, as in the case of surface manipulations using tip-based methods,[16-20,33-39] a break-junction technique,[40] separation of wires in contact,[41] or a pin-plate technique[42]). Moreover, recent theoretical predictions[16-20,43,44] and experimental observations[4-10,17,33-42] have revealed remarkable properties

of such junctions, particularly three-dimensional nanometer scale wires, which are of fundamental and of potential technological interest in the area of tribology as well as for miniaturization and very large scale assembly and integration of electronic devices. These findings include the following: structural characteristics (i.e., crystallinity);[16,17,19] mechanical response,[16,17,35,36,38] characterized by ideal critical yield stress values, with elongation occurring through a sequence of plastic stress accumulation and relief stages associated with ordered and disordered atomic configuration of the wires, and protrayed in oscillatory behavior of the pulling force; electronic transport[33,35,37,39-42] exhibiting room temperature conductance quantization as well as possible transition to a localization regime in sufficiently long wires;[35] and predictions of magnetotransport effects,[44] including magnetic switching and magnetic blockade,[45] occurring through the shifting of electronic energy levels in nanowires by an applied longitudinal magnetic field.

For metallic systems, consisting of a clean gold substrate and a nickel tapered and faceted tip (and for the reverse situation, i.e., a nickel surface and a gold tip), simulations revealed[17] the onset of an instability as the tip approaches the sample to a distance of ~4 Å, causing a jump-to-contact (with gold atoms displacing about 2 Å in about 1 ps) and formation of adhesive bonding between the two materials, driven and accompanied by atomic-scale wetting of nickel by gold atoms, due to differences in their surface energies. Furthermore, it was found that detraction of the tip from the surface after contact, results in a significant inelastic deformation of the sample exhibiting ductile extension, formation of a connective neck of atomic dimensions and eventual tear, yielding upon separation a gold-coated nickel tip and a damaged gold surface.

These phenomena, which were observed also in simulations involving indentations of the substrate[17] (i.e., penetration of the tip into the surface), exhibiting transitions from elastic to plastic mechanical response of metals and formation of extended atomically thin crystalline connective wires (see Figure 1), are portrayed by marked hysteresis in the calculated force-versus-distance relation between the interacting materials bodies upon lowering and lifting of the tip from the surface (i.e., the force records do not track each other for the two processes, see Figure 2). Furthermore, the simulations revealed the nature of the elongation process of such ordered crystalline atomic-scale junctions, consisting of straining and yielding stages occurring with a periodicity of the interlayer spacing in the wire, and being reflected in periodic oscillations in the recorded force (see Figures 1 and 2, recorded in a simulation[17] of a nickel tip slightly indenting a Au(001) surface, and subsequently retracted from it). In each elongation stage, atoms in layers (mainly in the vicinity of the narrowest part of the junction) respond first via accumulations of stress accompanied by the occurrence of strained configurations of the wire (which remains ordered in atomic layers, though with increasing nonuniformity of the interlayer spacings).

Insight into the process can be gained by consideration of the second invariant of the deviatoric stress tensor, J_2, which is related to the Von Mises strain-energy criterion for the onset of plastic yielding.[10] Examination of this quantity shows that gradually increases during the strain accumulation process, reflecting the increase in the stored strain energy. Additionally we found[17] that the maximum of $J_2^{1/2}$ is localized about a narrow region around the periphery in the strained neck (Figure 3). Upon reaching

(29) Landman, U.; Luedtke, W. D.; Ouyang, J.; Xia, T. K. *Jpn. J. Appl. Phys.* **1993**, *32*, 1444.

(30) Landman, U.; Luedtke, W. D. *MRS Bull.* **1993**, *17* (5), 36.

(31) Ryckaert, J. P.; Bellemans, A. *Discuss. Faraday Soc.* **1978**, *66*, 95.

(32) Xia, T. K.; Ouyang, J.; Ribarsky, M. W.; Landman, U. *Phys. Rev. Lett.* **1992**, *69*, 1967.

(33) Pascual, J. I.; Mendez, J.; Gomez-Herrero, J.; Baro, A. M.; Garcia, N.; Binh, Vu Thien *Phys. Rev. Lett.* **1993**, *71*, 1852.

(34) Pascual, J. I.; Mendez, J.; Gomez-Herrero, J.; Baro, A.; Garcia, N.; Landman, U.; Luedtke, W. D.; Bogachek, E. N.; Cheng, H.-P. *Science* **1995**, *267*, 1793.

(35) Pascual, J. I.; Mendez, J.; Gomez-Herrero, J.; Baro, A. M.; Garcia, N.; Landman, U.; Luedtke, W. D.; Bogachek, E. N.; Cheng, H.-P. *J. Vac. Sci. Technol., B* **1995**, *13*, 1280.

(36) (a) Agrait, N.; Rodrigo, J. G.; Vieira, S. *Phys. Rev. B* **1993**, *47*, 12345. (b) Agrait, N.; Rodrigo, J. G.; Vieira, S. *Phys. Rev. B* **1995**, *74*, 3995.

(37) Olesen, L.; Laegsgaard, E.; Stensgaard, I.; Besenbacher, F.; Schiotz, J.; Stoltze, P.; Jacobsen, K. W.; Norskov, J. N. *Phys. Rev. Lett.* **1994**, *72*, 2251.

(38) Kuipers, L.; Frenken, J. W. M. *Phys. Rev. Lett.* **1993**, *70*, 3907.

(39) Smith, D. P. E. *Science* **1995**, *269*, 371.

(40) Krans, J. M.; van Ruitenbeek, J. M.; Fisun, V. V.; Yanson, I. K.; de Jonhg, L. J. *Nature* **1995**, *375*, 767, and references to earlier work therein.

(41) Costa-Kramer, J. L.; Garcia, N.; Garcia-Mochales, P.; Serena, P. A. *Surf. Sci.* **1995**, *342*, L1144.

(42) Landman, U.; Luedtke, W. D.; Salisbury, B. E.; Whetten, R. L. Submitted to *Phys. Rev. Lett.*

(43) Bogachek, E. N.; Zagoskin, A. M.; Kulik, I. O. *Fiz. Nizk. Temp.* **1990**, *16*, 1404; *Sov. J. Low Temp. Phys.* **1990**, *16*, 796.

(44) Scherbakov, A. G.; Bogachek, E. N.; Landman, U. *Phys. Rev. B* **1996**, *53*, 4054.

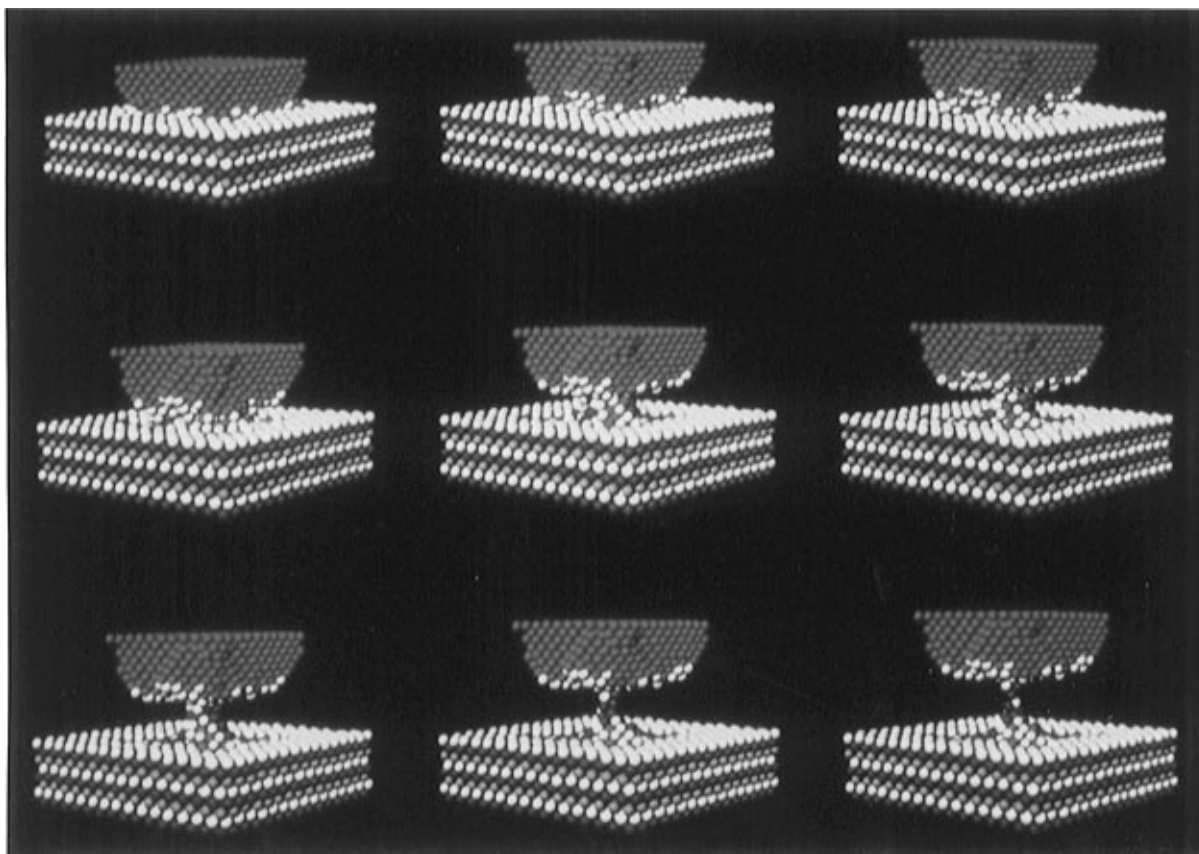(45) Bogachek, E. N.; Scherbakov, A. G.; Landman, U. *Phys. Rev. B* **1996**, *53*, 13246.

Figure 1. Sequence of atomic configurations starting from a Ni tip indented in a Au(001) substrate (top left) and during the process of retraction of the tip (from left to right) accompanied by formation of a connective solid gold junction, and culminating in a junction of atomic dimensions (bottom right). The MD simulations[17] were performed at $T = 300$ K. Red balls represent tip nickel atoms.
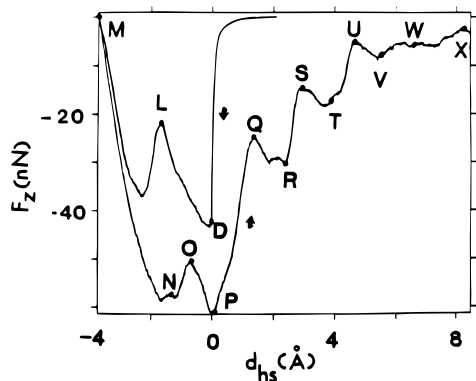

Figure 2. Force on the tip atoms, F_z, versus tip-to-sample distance, recorded in a MD simulation[17] of a Ni tip interacting with a Au(001) surface at 300 K. The simulation describes the tip approach to the surface, jump-to-contact (point D), indentation (points D, L, M), and subsequent retraction (points M, N, P, ..., X) of the tip from the surface. Note the marked hysteresis in the force upon retraction, and the oscillatory variations during elongation of the solid junction. d_{hs} denotes the distance between the rigid tip-holder assembly and the substrate (d_{hs} is normalized to zero at the jump-to-contact point, marked D). The capital letters denote the actual distances, d_{ts}, between the bottom part of the Ni tip and the top of the Au surface: D = 3.8 Å, L = 2.4 Å, M = 0.8 Å, N = 2.6 Å, O = 3.0 Å, P = 3.8 Å, Q = 5.4 Å, R = 6.4 Å, S = 7.0 Å, T = 7.7 Å, U = 9.1 Å, V = 9.6 Å, W = 10.5 Å, and X = 12.8 Å.

a critical maximum value of about 3 GPa (occurring for states at the end of the intervals marked OP, QR, ST, and UV in Figure 2) each of the straining stages is followed by a shorter atomic disordering and rearrangement period culminating in the formation of an added layer, with a relief of the accumulated stress and restoration of a higher degree of order in the wire. Consequently, each such
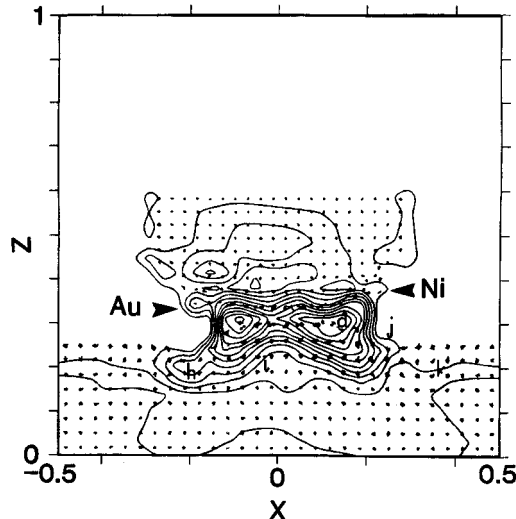

Figure 3. Contours of the Von Mises' shear stress ($J_2^{1/2}$) corresponding to the configuration marked T in Figure 2 (that is, just before the structural transformation from a two-layer junction to a three-layer one. The proximal interfacial layers of Ni and Au are marked by arrows. The maximum contours (2.9 GPa, marked a) occur on the periphery of the neck (X, Z) = (± 0.1, 0.3). The increment between contours is 0.2 GPa. The contours marked h, i, j, and k correspond to 1.1, 0.9, 0.7, and 0.5 GPa, respectively. Distance along X and Y in units of X = 1 and Z = 1 corresponding to 61.2 Å.

elongation-necking stage results in a more extended crystalline junction (in increments of the order of the interlayer spacing in the junction, i.e., ~2 Å) of a smaller cross-sectional neck area. It is of interest to note that from these calculations, as well as from evaluation of the normal pressure during the transformation, we predicted[17]
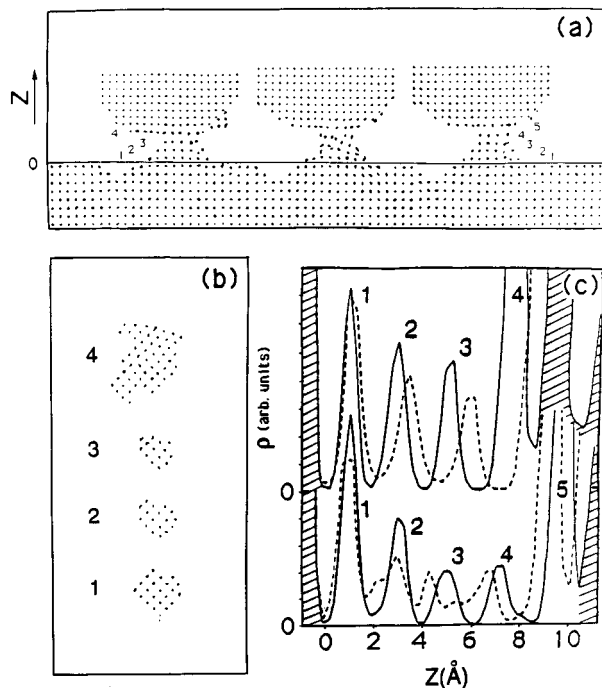
Figure 4. (a) Side views of atomic configurations obtained from short-time trajectories during a MD simulation[17] of a Ni tip slightly indented into, and then retracted from, an Au(001) surface at 300 K. On the left, a four-layer ordered gold junction formed between the tip and the substrate (the fourth layer of the junction coats the bottom of the tip); the middle configuration demonstrates disorder in the junction during elongation, culminating in the five-layer ordered junction shown on the right. (b) Top views of the in-layer atomic arrangements corresponding to the four-layer ordered wire. (c) Profiles of atomic densities plotted versus distance (Z) along the axis of the wire. The solid lines at the top and bottom correspond to the four-layer and five-layer ordered junctions, respectively (i.e., left and right configurations in (a)). The dashed line at the top part corresponds to the four-layer strained configuration and the one at the bottom to the disordered structure (middle configuration in (a)) which developed during the elongation process. Hatched regions represent Au substrate ($Z < 0$) and Ni tip layers.

that the yield strength of such nanowires is about 2−3 GPa, which is an order of magnitude larger than the macroscopic yield strength of Au (~200 MPa),[46] and is comparable to the theoretical value for Au (1.5 Gpa) in the absence of dislocations.[46] This prediction has been confirmed by recent experiments.[36b] The mechanical "ideal" nature of the nanowires can be related to their characteristic small dimensions and the inability to support dislocation sources[47] (e.g., Frank-Read sources[48]).

To illustrate the elongation process, we show in Figure 4a side views of atomic configurations, starting from a layer-ordered junction containing four atomic layers (see the corresponding intralayer atomic arrangements shown in Figure 4b) and ending with a longer layer-ordered junction containing five layers, along with a structure during the intervening disordered stage.[17,34] Corresponding plots of the atomic density profiles along the normal axis (Z) of the junction shown in Figure 4c illustrate the atomic distributions in the initial and final ordered stages of the junction as well as during the straining and disordering stages of the transformation.

During elongation the wire evolves through atomic configurations with various degrees of order and disorder.
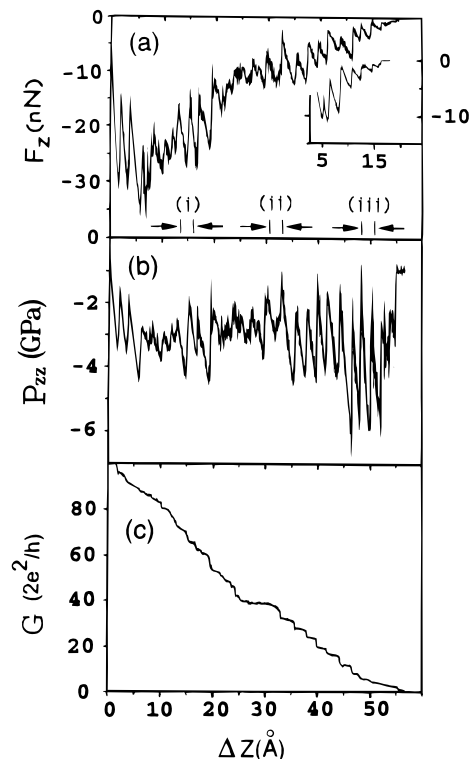
(46) Kelly, A.; MacMillan, N. H. *Strong Solids*; Clarendon: Oxford, 1986.

(47) Herring, C.; Galt, J. K. *Phys. Rev.* **1952**, *85*, 1060.

(48) Hall, D. *Introduction to Dislocations*; Pergamon: Oxford, 1975.

Figure 5. Force (F_z, in nN, shown in a), axial component of the stress tensor (P_{zz}, in GPa, shown in b) and calculated conductance (G, in unit of $2e^2/h$, shown in c), plotted versus displacement (Δz, in Å) obtained from room-temperature MD simulations of the elongation of a large (111)-oriented gold wire (initially equilibrated as a 30-layer wire with a ~17 Å radius of its narrowest cross section). The displacement intervals marked i−iii correspond to those for which atomic configurations are shown in Figure 6a−c, respectively. Shown in the inset is the force (F_z, in nN) recorded in a separate simulation of the elongation process of a smaller Au(111) wire (equilibrated initially as a 16-layer wire with a radius of ~10 Å at its narrowest cross section). The displacement scale for the shorter wire was positioned with respect to that of the longer one such that at its start the radii of the narrowest cross sections of the two wires achieved very close values. This comparison serves to illustrate the invariance of the properties of nanowires formed during elongation of junctions with respect to the initial sizes of the junctions.

Note that even at the ordered stages, which exhibit crystalline-like atomic layers along the axis of the junction, the shapes of the layers are rather irregular (see Figure 4b), resulting in a solid wire with a surface roughness of a few angstroms, comparable to the wavelength of the conduction electrons in such wires (~4 Å). While such an aspect of disorder may not greatly affect the mechanical characteristics, it can influence electronic transport processes.

It is natural to inquire whether the phenomena described above are restricted to junctions of small dimensions such as those considered in the early simulations and about the size-evolutionary patterns of the properties of such materials structures.[42,49] To this end we show in Figure 5 physical characteristics obtained via simulations of the room temperature elongation processes of larger junctions. In these simulations two crystalline gold wires oriented with the (111) direction parallel to the axis of the wire were used: (i) a long wire containing 8030 atoms, 5742 atoms treated dynamically and equilibrated initially as a 30-layer wire with the remaining atoms comprising Au(111) substrates of two layers each supporting the top and bottom of the wire, and (ii) a shorter wire (see inset

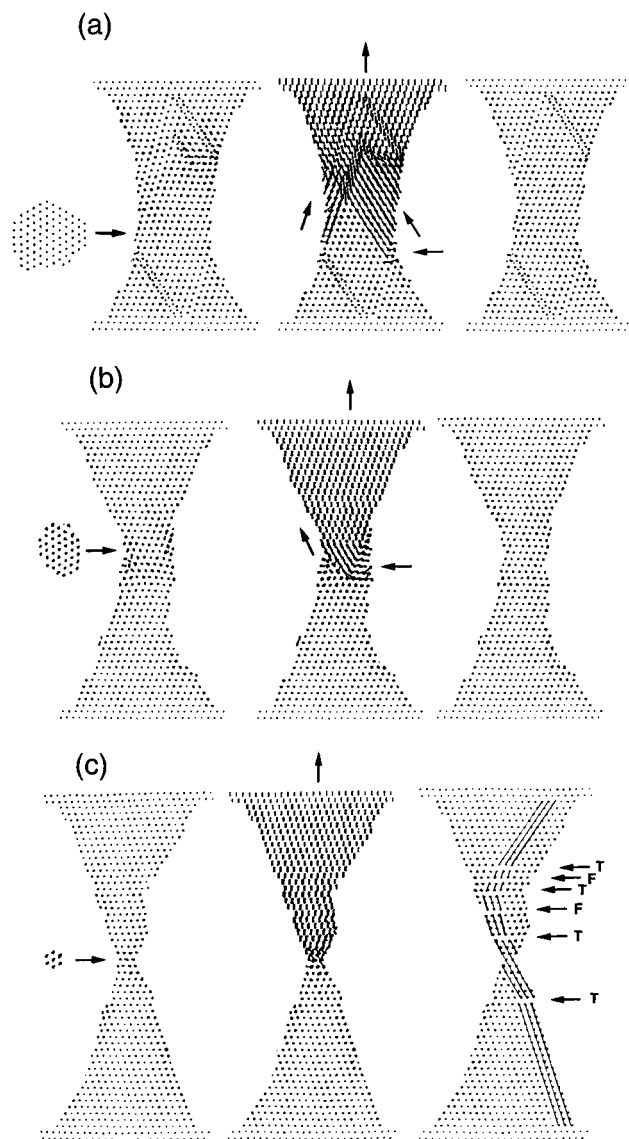(49) Luedtke, W. D.; Landman, U. To be submitted for publication.

Figure 6. Side views of atomic configurations and short-time trajectories in 5 Å thick vertical slices through the long wire, recorded (a–c) during the elongation stages i–iii marked in Figure 5, respectively. In each stage the left and right frames correspond to before and after configurations, and the central one corresponds to the brief structural transformation stage; the arrows in the middle frames of (a) and (b) denote the glide directions. For the final configuration in (c) fault (F) and twin (T) planes are marked (lines along atomic rows are drawn to guide the eye). Included also in (a–c) are top views of the narrowest cross sections of the wires, before the elongation step.

in Figure 5a), consisting of 3273 atoms, 1600 atoms treated dynamically and equilibrated initially as a 16-layer wire and the rest comprising Au(111) static substrates. In Figure 6 we display atomic configurations and short-time trajectories recorded at selected stages of the elongation process of the longer wire (Figure 6a–c corresponding to the intervals marked i–iii in Figure 5a). From these simulations the following main observations can be made:

(i) Underlying the oscillatory sawtooth pattern of the forces in Figure 5a and the corresponding behavior of the axial component of the stress tensor (calculated at the narrowest region of the wire) shown in Figure 5b are the atomistic mechanisms of elongation of the wire. As aforementioned these processes occur via a succession of alternating stress accumulation and relief stages, during which the wire undergoes plastic structural transformations. The atomic structure of the wire is crystalline-ordered in nature during most of the evolution of the wire

(though strained during the stress accumulation stages); see for example the left and right configurations in Figure 6a–c. These ordered states of the wire are interrupted rather abruptly by brief transformation stages during which the wire is locally disordered. For wires as thick as those used in this study, these transformations involve multiple-glide processes primarily on (111) glide planes (see Figure 6a–c; in particular note the middle configurations in Figure 6a and Figure 6b recorded during the glide stage, where the glide planes are denoted by arrows). The structural transformations lead to elongation of the wire. Accompanying these processes are variations in the cross sectional areas and shapes of the wire; note that the intersection of the glide planes with the periphery of the wire can cause areal and shape changes even in locations other than the narrowest neck region, which in some circumstances can lead to a double-constriction structure. Additionally, for sufficiently thin wires successive narrowings are localized at the narrowest region (typically for wires with diameters ∼20 Å, depending on the ratio of the neck radius to the global axial radius of curvature of the wire), while for thicker ones, i.e., at the earlier stages of pulling of a thick wire, narrowings may occur occasionally at thicker regions, leaving the area and shape of the narrowest constriction essentially unaltered.

Since ballistic conductance through the wire is determined mainly by the dimensions and shape of the narrowest constriction (i.e., the number of conducting channels is given by the number of transverse electronic states at this region, and their degeneracies;[43] see ref 44 and citations to earlier studies therein), such structural occurrences can lead to the development of extended plateaus in the conductance measured versus the extent of elongation. Indeed, such an extended plateau is seen in Figure 5c (in the interval 25 Å $\leq z \leq$ 32.5 Å), where we display the conductance of the wire calculated via a semiclassical modification of Sharwin's expression.[50] Furthermore, double-constriction structures may also influence the conductance characteristics (e.g., when the two constrictions in a doubly-constricted wire are well separated from each other the total resistance of the wire is that due to two constrictions in series resulting in a smaller conductance).

We also observe that the structural transformations of the wire can lead to the generation of stacking faults and/or twin-boundaries (see for example Figure 6a). Such defects may anneal during the structural evolution of the pulled wire (compare Figure 6a and Figure 6b), and some may be present even in the ultimate stretched nanowire (see Figure 6c where faults and twin boundaries, denoted by F and T, respectively, are seen). Such defects may also influence the ballistic transport of electrons through the wire. Finally, we note that the local curvature of the axial shape of the pulled wire may be very different from the overall average curvature (see in particular Figure 6c). The local curvature at the vicinity of the narrowest constriction of the wire influences the tunneling contribution to the transmission through the constriction and is of importance in estimating the conductance through such wires (see ref 44 and citations of earlier studies therein).

(ii) The force and axial pressure traces (Figure 5a,b) recorded during elongation of a large wire (equilibrated initially with a constriction radius of 17 Å) exhibit a regular pattern (almost equally spaced oscillations with a period of ∼2.5 Å; the interlayer distance between (111) layers is ∼ 2.35 Å) at the later stages of elongation (i.e., for $\Delta z \geq$ 32.5 Å, when the radius of the narrowest constriction in

(50) Fal'ko, V. I.; Lesovik, G. B. *Solid State Commun.* **1992**, *84*, 835. Torres, J. A.; Pascual, J. I.; Saenz, J. J. *Phys. Rev. B* **1994**, *49*, 16581.

the wire achieved a value of ~10 Å). On the other hand, prior to this stage ($\Delta z \le 32.5$ Å, corresponding to a thicker wire) the force and stress patterns are more irregular, with large variations in the oscillation amplitudes and periods. Underlying this difference in behavior is the observation that when the wire is thicker, accumulated stresses induced by pulling may be distributed in various regions of the wire and a large number of glide planes (mainly (111)) with variable dimensions can be active. This leads to a broad variation of the critical stress values from one elongation stage to another. As the wire thins down the stresses concentrate at the narrowest region of the wire and the number of active glide planes decreases, resulting in a more regular pattern of the forces and stresses. This is reflected also in the calculated conductance (Figure 5c) which shows a much more regular pattern past $\Delta z \approx 32.5$ Å, characterized by well-defined plateaus and step-rises. Note in this context the small slopes of the semiclassically calculated conductance plateaus originating from variation of the uniaxial strain during the stress accumulation intervals (between yield, i.e., transformation, stages) which is accompanied by continuous contraction of the wire's cross-sectional areas; such slopes have been observed experimentally[42].

(iii) A most interesting result of the simulations pertains to the "universal" nature of the mechanical and electrical properties of junctions. It has been observed already from the early simulations[17] that nanometer scale wires are formed at the latter stages of elongation irrespective of the initial size of the contact. This is further illustrated in Figure 5a where the force vs elongation curves for two wires of different initial dimensions are compared starting from the corresponding elongation stages when the radii of the narrowest cross sections of the two wires become very close to each other (~8 Å). The similarity between the force curves for the two wires (also reflected in other mechanical characteristics and in the calculated conductance curves,[49] not shown here for the shorter wire) confirms formation of nanowires of similar nature, irrespective of the previous history of the junction. Indeed, such considerations guided recent experiments where quantized conductance in nanowires has been measured via separation of the contact between two macroscopic bodies.[41,42]

These theoretical predictions have been verified by recent experimental studies using atomic force microscopy (AFM) for investigations of the mechanical properties of atomic-scale solid junctions,[36] measurements at room temperature of electronic conductance quantization in atomically thin gold wires,[33-35,37,41,42] including a transition to a localization regime in wires whose extension (longer than 100 Å) is larger than the localization length,[34] and measurements of reversible conductance behavior in extension—compression cycles of nanowires using a pin-plate technique.[42]

In the conductance experiments,[34] contact between the tip and the substrate is produced either by applying a voltage pulse or by indentation, starting from typical STM tunnel conditions. Once the contact is produced as indicated by the electrical current flowing between the two electrodes, it was elongated by retracting the tip slowly (~1 Å/s). Gold evaporated onto mica and Au(110) single crystals was used as samples, and Pt/Ir and gold tips were employed interchangably (the results are insensitive to the kind of tip used; most likely, the Pt/Ir tip apex is covered with gold atoms once the tip touches the sample). Since the wires are more easily formed in air, measurements were performed under ambient conditions. However, similar results were obtained in ultrahigh vacuum. Experiments were performed on a large number of wires
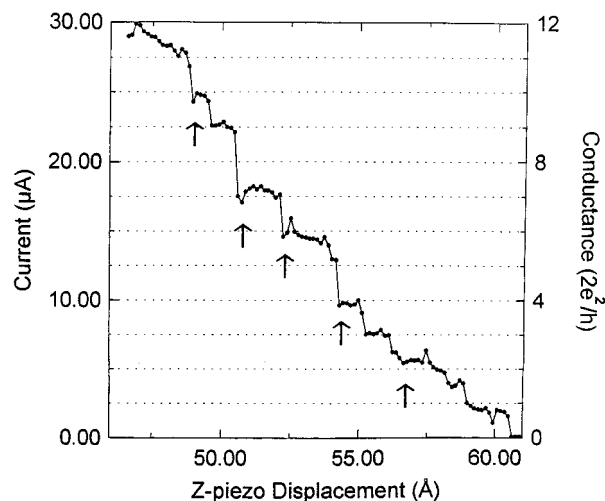

Figure 7. Current and conductance in a short wire during elongation, exhibiting room-temperature conductance quantization steps.[34] Dashed lines denote $2e^2/h$ intervals. Arrows indicate dips, associated with disordered elongation stages, becoming somewhat less pronounced toward the breaking of the wire.

(both short and long ones). Typical data are shown in Figure 7 for the conductance of a short wire (~50 Å) produced by bringing a Pt/Ir tip to contact with a gold surface at room temperature and subsequently elongating the contact slowly by retracting the tip (a constant bias voltage of 32 mV was applied during the process). The voltage was kept constant during the measurements by using a low gain I–V converter.

The appearance of room-temperature quantized conductance in the short wires and its persistence (see Figure 7 where nine steps of height $2e^2/h$ or $2(2e^2/h)$, with a period $d \sim 2$ Å, the interlayer spacing in the material, are seen) are quite remarkable, particularly in view of the known sensitivity of conductance quantization to the presence of disorder (which in our wires includes surface roughness, and disorder occurring between the intermittent layer-ordered stages, see Figures 4 and 6) and the shape of the cross section in the narrow region of the junction.[44] This implies that overall, wires in this length regime maintain a sufficient degree of crystalline order (see Figures 1, 4, and 6) to sustain quantization of the conductance. Furthermore, significant insights into the microscopic mechanism of the elongation process and nature of disorder in the wire are provided by the observation of dips (local conductance minima) which tend to accompany the quantized conductance steps (see Figure 7) and can be associated with electron scattering caused by the enhanced structural disorder developing toward the completion of each of the discrete elongation stages of the wire (see Figures 4 and 6). The rapid rise in the conductance following each dip indicates restoration of a higher degree of order in the pulled wire subsequent to the disordering—rearrangement elongation stage. In addition, the variability in the conductance quantization step-height (one or two $2e^2/h$ units) and the above-mentioned occasional occurrence of two successive steps in an elongation interval of combined length d (see Figure 7), may originate from factors influencing the quantization of transverse electronic stages (channels) in the wire (these include accidental degeneracies of transverse electronic modes, irregular layer shapes, and most likely the occurrence of intermediate atomic configurations during the elongation process which satisfy the condition for closing of a conductance channel; see also our discussion in the context of Figures 5 and 6). These observations support a correlation between the measured patterns and
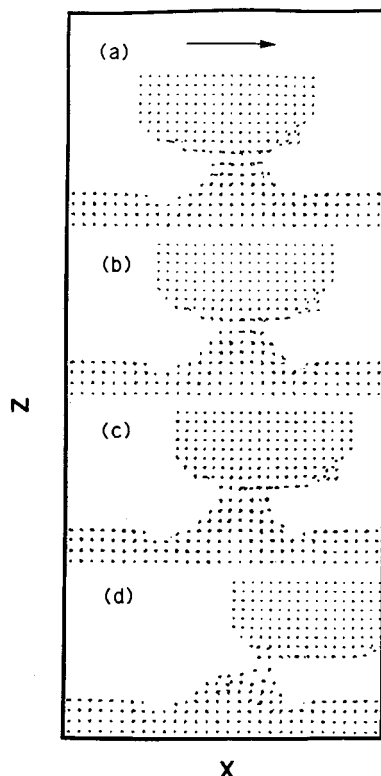
Figure 8. Side-view atomic configurations of a four-layer gold junction between a nickel tip and a gold surface (see Figure 4) recorded during a simulation of sliding of the tip with respect to the surface in the *x* direction with a velocity of 2 m/s, at *T* = 300 K. In this simulation the distance between the tip holder and the bottom of the substrate was kept constant, i.e., an AFM constant height mode. Sliding shear occurs between the gold layer wetting the nickel tip and the layer below it.

the aforementioned periodic layerwise order−disorder elongation mechanism of the wire.[17]

Starting from the four-layer neck configuration shown in Figure 4a, sliding of the tip assembly in the *x* direction, with a velocity of 2 m/s, resulted in shearing of the connective junction (see Figure 8). The shear of the gold junction occurred between the gold layer adherent to the nickel tip and the layer underneath it, and proceeded in a "ratcheting" (atomic-scale stick−slip) manner, reflected in the recorded forces on the tip which oscillate as atomic rows in the two layers pass each other (Figure 9). From the magnitude of the forces and the contact area between the sliding layers we estimate the shear strength of the junction as ∼2 GPa. The magnitude of the frictional shear resistance depends on the sliding direction and registry between the sliding layer. In addition, simulations of tribological phenomena when the two interfacing materials slide with respect to one another involving crystalline ionic solid (CaF_2) and semiconductors (Si) revealed atomic-scale stick−slip (i.e., oscillatory bonding and bond-breaking behavior),[20,51] tip shearing, and interfacial material transfer,[51] and the results have been used to calculate the critical yield-stress of sheared ionic interfaces and their temperature dependence and correlate these predictions with tribo-testing measurements.

(b) Liquid Junctions. Molecular dynamics simulations of the nanotribology of interfacial liquids and confined films aim to explore the relation between the physical properties and response of model lubricants and their molecular characteristics, such as chain lengths and molecular structural complexity (for example, straight
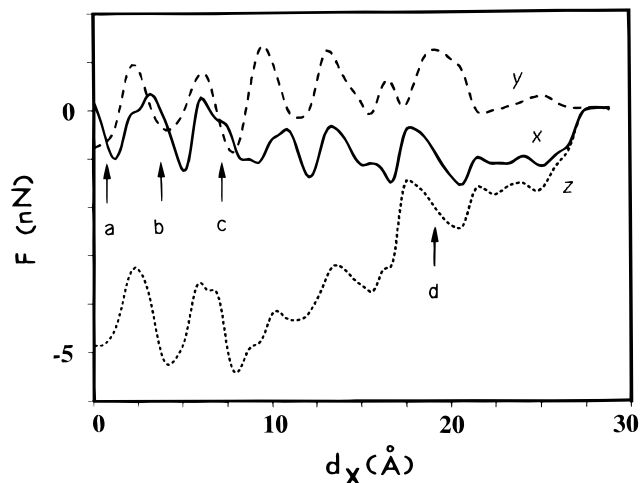

Figure 9. Components of the forces in nanonewtons on the tip holder, recorded during the sliding simulation, plotted versus the sliding distance d_x (in Å). The points marked a−d, correspond to the respective atomic configurations shown in Figure 8. Note the rather regular oscillatory pattern of the forces (particularly F_x and F_y associated with the interlayer ratcheting sliding process.

versus branched chains). Such simulations of alkanes and self-assembled boundary-lubricant systems have revealed liquid-junction formation,[18,29,30] inhibition of the generation of solid junctions,[51] and layering phenomena and in-plane ordering owing to confinement[18,21,22] and have shown how self-assembled monolayers respond to compression by a tip or flat surface.[52−55] Simulations have also been performed of collapse and drainage mechanisms of confined molecular films and their dependence on the strength of bonding to the substrate,[21] the dependence of thin-film viscosities on the shear rate[56] and the origin of stick−slip phenomena in shear-induced "solidification" and melting,[23,26,57] mechanisms of cavitation in thin molecular liquid films induced by fast motion of immersed tips,[30] and correlations between structural and dynamical transformations in lubricating films with force−distance characteristics.[18,29,30] Simulations of thin-film model lubricants made of mixtures of long-chain molecules of different lengths have illuminated the molecular mechanisms of preferential segregation of the longer-chain molecules at the liquid−solid interface.[58]

3. Nano-elastohydrodynamics

Underlying the development of the theory of elastohydrodynamic lubrication (EHL)[5,6] was the observation that when two nonconforming solid surfaces come into contact in the presence of a liquid lubricant (or when two asperities of nominally conforming surfaces, under conditions of boundary lubrication, come together), the pressure developed in the contact zone may achieve such high values that local elastic deformations of the surfaces must be included in proper treatments of lubrication of the tribosystem. The subsequent development of micro-EHL and numerical algorithms[5,6] allowed investigators to focus on lubrication processes involving individual surface irregularities (asperities) and have aided the design of

(51) Landman, U.; Luedtke, W. D.; Ringer, E. M. *Wear* **1992**, *153*, 3.

(52) Callaway, M.; Tidesley, D. J.; Quirke, N. *Langmuir* **1994**, *10*, 3350.

(53) Tupper, K. J.; Colton, R. J.; Brenner, D. W. *Langmuir* **1994**, *10*, 2041.

(54) Tupper, K. J.; Brenner, D. W. *Langmuir* **1994**, *10*, 2335.

(55) Karaborni, S. *Phys. Rev. Lett.* **1994**, *73*, 1668.

(56) Thompson, P. A.; Grest, G. S.; Robbins, M. O. *Phys. Rev. Lett.* **1992**, *68*, 3448.

(57) Thompson, P. A.; Robbins, M. O.; Grest, G. S. In ref 16a, p 127.

(58) Xia, T. K.; Landman, U. *Science* **1993**, *261*, 1310.

machine elements and bio-tribological systems[2,7] of improved efficiency and durability. Inherent to these continuum models are certain assumptions which are used as input into the calculations. These include constitutive relationships such as rheological properties of the lubricant film (Newtonian or non-Newtonian viscosity laws, as well as pressure and temperature variations of the viscosity) and mechanical response characteristics of the bounding surface materials (substrates and asperities), as well as imposed interfacial liquid−solid boundary conditions.

Asperity−asperity collisions, formation and subsequent breakage of interfacial adhesive junctions, and shear-induced rheological transformations in highly confined fluids are among the most fundamental processes in tribology as well as boundary and thin-film lubrication.[3,14] To investigate the atomic and molecular origins of such processes in morphologically nonuniform lubricated narrow junctions sheared at high velocities, we have used MD simulations, thus extending micro-EHL investigations to the nanoscale regime which is beyond the range of applicability of continuum-based models.[59] As model systems we used thin films of hexadecane (n-$C_{16}H_{34}$) confined between two gold substrates exposing (111) surfaces (that is, Au(111)). Topographical nonuniformities (asperities) were modeled by flat-top pyramidal gold structures of height h_a from the underlying gold surface, extending a finite length in the x direction and over the whole simulation cell in the y direction (that is asperity ridges; see views along the y direction in Figure 10).

For each of our systems a typical simulation consisted of $(4 \times 10^5)\Delta t$ (where the integration time step $\Delta t = 3.06 \times 10^{-15}$ s), i.e., 1.2 ns, past a prolonged equilibration stage. In simulations of shear-induced flow, the solid surfaces were kept at constant separation (chosen to correspond to an initially vanishing average normal load) and were translated along the x axis in opposite directions, with the top and bottom surfaces moving with a constant velocity of ± 5 m/s (a relative sliding velocity $V = 10$ m/s). In these simulations the alkane molecules and the gold atoms of the asperities were treated dynamically. The simulations were performed isothermally, at a temperature $T = 350$ K, via scaling of intramolecular velocities in 50 Δt intervals.

To explore the dependence of structure, dynamics, and flow on the characteristics of the lubricated junctions, we show results for two lubricated systems; (I) consisting of 243 hexadecane molecules with the separation between the gold surfaces $S = 23.2$ Å, the height of each of the asperities $h_a = 9.3$ Å, and thus the separation between the asperity tops $\Delta h_{aa} = S - 2h_a = 4.6$ Å, which we refer to in the following as the near-overlap case; and (II) consisting of 201 molecules, with $S = 21.3$ Å, $h_a = 14$ Å, and $\Delta h_{aa} = -6.7$ Å referred to as the overlap case (see Figure 10). In describing our results, we denote by d_{aa} the distance along the x direction between the leading edges of the opposing asperities. For each system the simulations of sliding followed equilibration with the asperities well distances from each other, such that steady state flow could be established before the onset of effects caused by lubricant confinement in the interasperity region.

(a) Layering, Friction Force Oscillations, and Deformations. Atomic and molecular configurations of the two simulated systems, recorded in each case at selected times during the shearing process, are displayed in Figure 10. The main patterns illustrated by these configurations are the evolution of liquid layered structures in the region between the colliding asperities and

the severe deformations of the asperities for the cases of near-overlapping (Figure 10a) and overlapping (Figure 10b) asperity heights. It is particularly noteworthy that while in all cases a certain degree of interfacial layering in the vicinity of the solid boundaries already exited at equilibrium and for large transverse separations between the asperities, the layering of the lubricant in the interasperity region was initially absent and developed dynamically as the asperities approached each other. Furthermore, the number of layers in that region evolved in each case in a quantized manner as successive layers were squeezed out of it when the asperities came closer together.

These atomic and molecular structural variations are portrayed in the behavior of the forces acting between the thin film molecules and the solid substrates, as well as by the intermetallic interactions between the two solid surfaces. As a demonstration we show in Figure 11 the time variation of the forces in the shear and normal directions (f_x and f_z, respectively) recorded during a simulation of the nearly overlapping system. Of particular interest are the oscillatory patterns in the forces prior to the collision between the asperities, whose characteristics correlate with the structural layering stages of the lubricating film (compare Figure 11 and Figure 10a; note that the marked minima in f_x and f_z, seen particularly clearly in f_x, correspond to successively decreasing discrete numbers of molecular layers in the interasperity region).

The new aspects revealed by our investigations are that molecular density layering and consequent solvation force oscillations can occur not only in liquids confined between smooth solid surfaces under equilibrium conditions as discussed in the previous section[14] but also under constant-velocity shear-flow conditions in a lubricated junction with nonuniform surfaces and that such oscillations, correlated with quantization of the number of lubricant layers in a localized region of the contact (that is the interasperity zone), can be exhibited both in the normal (f_z) as well as the tangential (f_x) forces. The implication of these observations (which we have made also for other simulated systems with different values for S) is that such oscillations in the force resisting the relative sliding motion (that is the friction force, f_x) may lead to stick−slip behavior in experiments where the sliding of the substrates (kept at constant normal separation) is driven via a connection through a spring element to a stage dragged at constant velocity (as in SFA measurements).

Another aspect revealed by the simulations[59] pertains to the crucial importance of the dynamical mechanical response of the substrates and in particular that of the irregularities (asperities), in determining the evolution and properties of sheared systems, as is illustrated through the atomic configurations shown in Figure 10, as well as the force and local stress plots shown for the near overlap system in Figures 11 and 12, respectively. For relatively large spacing between the asperity heights shear-flow accompanied by structuring of the lubricant occurs with no distortions of the metal surfaces. However, in the cases of nearly overlapping (Figure 10a) and overlapping (Figure 10b) surface irregularities, great densification and pressurization of the lubricant in the interasperity region occur, accompanied by significant increase of the effective viscosity in that region (detailed analyses of the rheological and dynamical characteristics indicate formation of a viscoelastic or elastoplastic zone, see below). These processes result in deformations of the gold asperities, much beyond the elastic response regime.

For the case of near asperity overlap (Figures 10a, 11, and 12) the gradually increasing confinement of the interasperity region is accompanied by the development

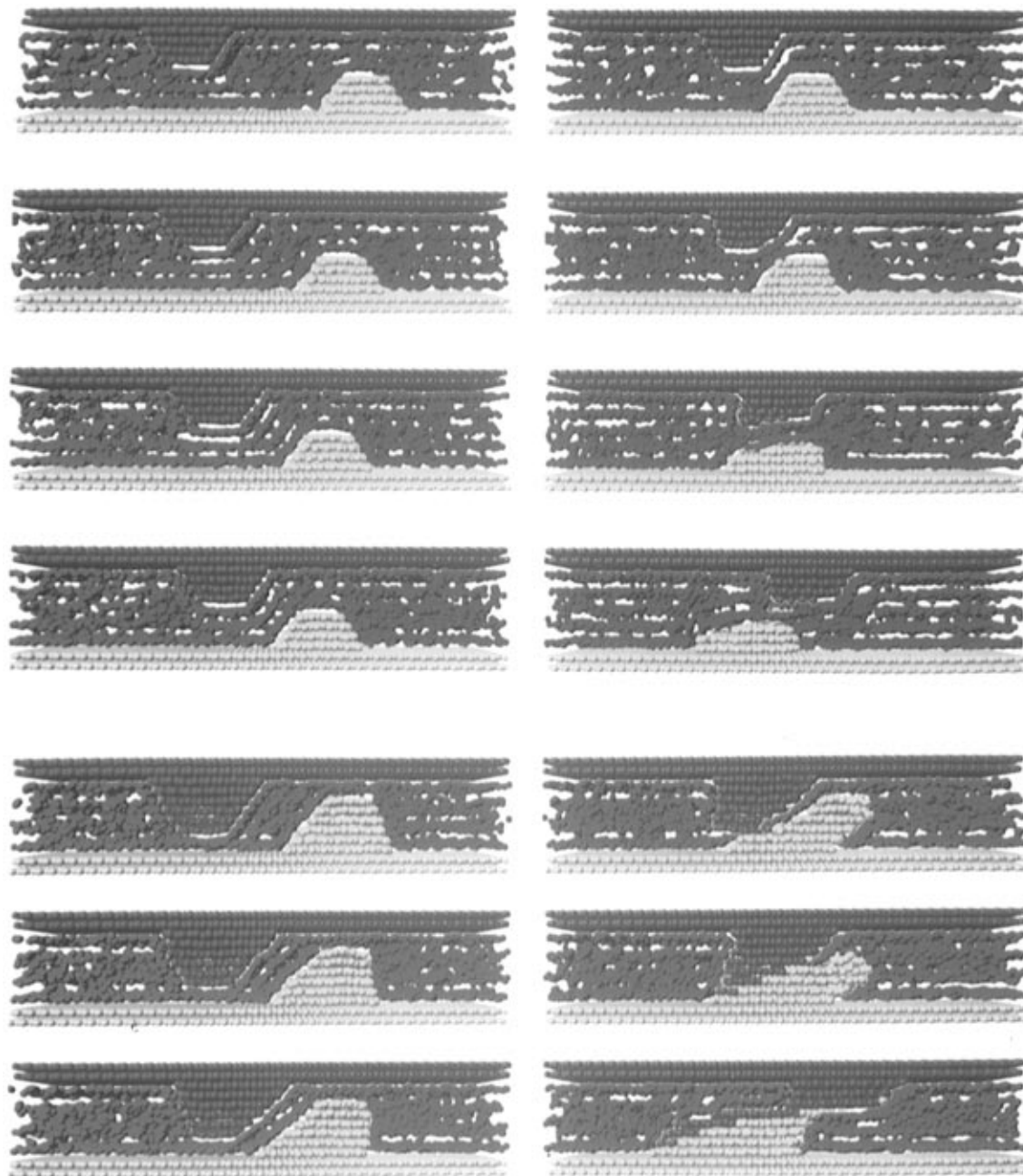(59) Gao, J.; Luedtke, W. D.; Landman, U. *Science* **1995**, *270*, 605.

Figure 10. Side views of atomic and molecular configurations recorded at selected times during MD simulations[59] of the sliding process of nonuniform gold Au(111) surfaces (yellow and red balls describing the bottom and top surfaces, respectively), lubricated by hexadecane molecules (the molecular segments are described by the green balls). The top surface translated in the horizontal, x, direction and the bottom one in the $-x$ direction, with a relative velocity of 10 m/s. The linear dimension of the system in the x direction is 115.4 Å. (a) Top four rows corresponds to the asperity near overlap system with the separation between the asperity heights $\Delta h_{aa} = 4.6$ Å. (b) The bottom three rows describe the asperity-overlap system with $\Delta h_{aa} = -6.7$ Å. The selected times (in ps) for the above systems are (in each case the system starts at the top left proceeding downward and ending at the bottom right): (a) 156, 250, 308, 351, 400, 461, 614, and 766; (b) 122, 184, 245, 398, 489, and 797. Denoting by d_{aa} the distance along the x direction between the leading edges of the approaching asperities, conversion of the above times to d_{aa} distances can be achieved by $d_{aa} = d_0 - 0.1t$, where $d_0 = 38.7$ Å (for a) and $d_0 = 18.7$ Å (for b) and t is in ps. Note layering in the interasperity zone for the two systems, and asperity deformations.

of transient local stresses in front of the moving asperities (in Figure 12 local stresses normal to the interfaces, τ_{zz}, and along the shear direction, τ_{zx}, are shown). Similar results were obtained for the overlapping-asperity case with even larger magnitudes of the stresses. The local shear and normal stresses which develop in the junction are of comparable magnitudes, with $\tau_{zz} > \tau_{xz}$ when the asperities come closer together (see $t = 585$ ps in Figure 12). Upon exceeding a limiting value of close to 4 GPa, these accumulated local stresses lead to severe deformations and structural transformations of the asperities, mediated by the intervening lubricant molecules, even

before the onset of direct intermetallic interactions (see Figures 10a, 11, and 12). In some locations along the asperity ridge (in the y direction) drainage of the lubricant molecules was complete when the sliding asperities passed over each other, leading to the formation of an intermetallic connective junction which sheared and eventually broke upon continued sliding, resulting in transfer of some metal atoms between the asperities. In this context we remark that in comparative simulations under the same conditions with no lubricant molecules in the junction, the magnitudes of the interaction between the asperities and the degree of deformation were found to be insignificant.
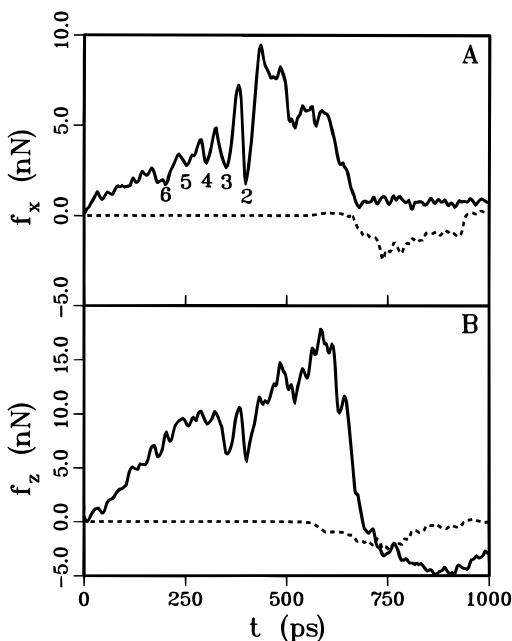
Figure 11. Total forces (in the *x* direction, f_x, and in the direction normal to the surfaces, f_z) on the gold solid surfaces from the alkane molecules (solid lines), plotted vs time, for the near overlap system (see Figure 10a; for conversion to interasperity distances, see caption). Intermetallic forces between the opposing solid gold surfaces, with an onset upon close approach of the asperities, are depicted by the dashed line. The numbers in f_x designate the "quantized" number of layers in the interasperity zone (see Figure 10a). Note the correlation between the force oscillations and the structural variations in the lubricant.[59]

Asperity deformations, complete lubricant drainage, growth of intermetallic junctions, shear-induced metal epitaxy, partial spreading via interlayer slip in the intermetallic junctions resulting in structural modifications of the surface topography (smoothing), and eventual rupture of such junctions are most pronounced for the case of overlapping asperities (see Figure 10b). The results for both this system and the near overlap one suggest that in addition to the aforementioned lubricant-mediated smoothing of surface roughness, oscillatory shear or cyclic relative motion of the surfaces may lead to materials fatigue, wear, and eventual failure due to repeated stress loading cycles of the surfaces.

For the near overlap system, we comment also on the occurrence of post-asperity-collision local rupture of the liquid film in the region between the departing asperities, resulting in the appearance of a nanoscale cavitated zone[30] (of a length scale of ~30 Å, and lasting for a period of over 100 ps). The appearance of such cavitated zones is associated with insufficient back flow of lubricant molecules into that region. The formation and consequences of cavitated zones in lubricating films, which are subjects of basic and technological significance, have been recently discussed in the context of micro-EHL simulations[60,61] of film breakdown as two rough surfaces slide against each other.

(b) Viscous and Waxy Dynamics. As aforementioned, shear-induced structural ordering and "phase changes" in confined thin lubricating films, and their rheological consequences, are among the unique features revealed via recent experiments[14b,62-67] and computer

simulations[22-26,59] on such systems. These phenomena, occurring during frictional sliding, are dynamical in nature (rather than being intrinsic equilibrium thermodynamic properties of the lubricant material) and depend not only on the temperature and pressure (or applied load) but also on the sliding velocity of the shearing surfaces, the interfacial coupling strength, and energy exchange and momentum transfer mechanisms between the lubricant molecules and the solid surfaces (in general it was found that at higher sliding velocities the film appears more solid-like).

The shear rheological response of lubricants under extreme load conditions has been a vexing problem in engineering studies of elastohydrodynamic contacts and led to much research and speculation over the past several decades.[68-75] These continuum-based investigations led to the development of several viscoelastic rheological models. Common to such treatments is the description of the lubricant by a "nonlinear Maxwell" model described by an equation of the form

$$\dot{\gamma} = \dot{\gamma}_e + \dot{\gamma}_v = \frac{d(\tau/G)}{dt} + \frac{\tau_r}{\eta} F(\tau) \qquad (1)$$

where $\dot{\gamma}$ is the total shear rate of the lubricant, τ is the stress, and $\dot{\gamma}_e$ is the "elastic" contribution (where G is the elastic shear modulus; in some treatments[70] it is taken out of the time derivative in eq 1). $\dot{\gamma}_v$ is the "viscous" contribution, η is the viscosity which is temperature and pressure dependent, and τ_r is a representative stress. The nonlinear viscous function $(\tau_r/\eta)F(\tau)$, expressing the relationship between the viscous shear rate and the shear stress (τ), may take different forms (e.g., the Eyring–Ree model[70] where $F(\tau) = \sinh(\tau/\tau_r)$; for another form of a limiting shear stress, see ref 75) and should reduce to the Newtonian limit τ/η when τ is small.

The relative significance of the two terms in eq 1 leads one to associate under various conditions different states and response regimes to sheared lubricants[68-77] (such as viscous fluids, "weak" solids, elastic, plastic, and elasto-plastic solids, and waxy and vitrified fluids). Such classifications are fascilitated by rewriting eq 1 in the form (assuming a weak dependence of G on time, or replacing it by an average value; see in this context ref 75)

$$\dot{\gamma}\eta = D \frac{d\tau}{dx^*} + \tau_r F(\tau) \qquad (2)$$

where $x^* \equiv x/l$, with l being a characteristic length in the

(60) Ai, X.; Cheng, H. S.; Zheng, L. *ASME J. Tribol.* **1993**, *115*, 102.
(61) Chang, L.; Jackson, A.; Webster, M. N. *Trib. Trans.* **1994**, *37*, 435.
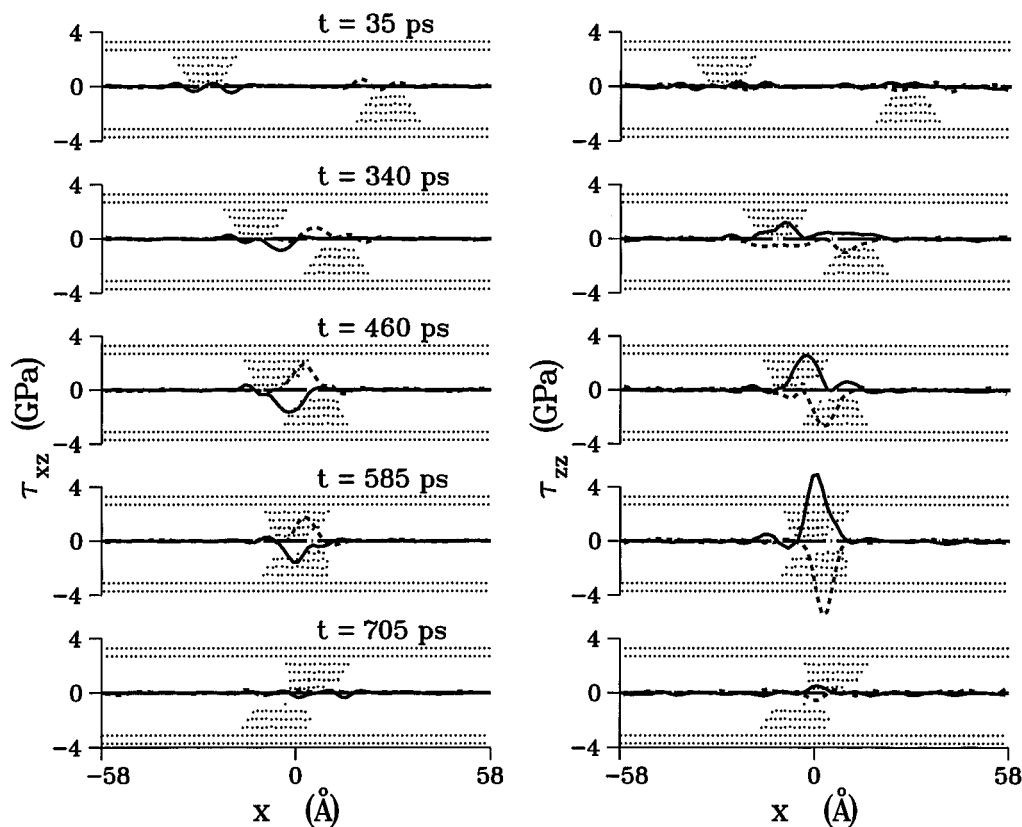(62) Granick, S. *Science* **1991**, *253*, 1374.

(63) Yoshizawa, H.; McGuiggan, P.; Israelachvili, J. N. *Science* **1993**, *259*, 1305.
(64) Yoshizawa, H.; Israelachvili, J. N. *J. Phys. Chem.* **1993**, *97*, 11300.
(65) Van Alsten, J.; Granick, S. *Phys. Rev. Lett.* **1988**, *61*, 2570.
(66) Hu, H. W.; Carson, G.; Granick, S. *Phys. Rev. Lett.* **1991**, *66*, 2758.
(67) Reiter, G.; Demirel, A. L.; Granick, S. *Science* **1994**, *263*, 1741.
(68) Johnson, K. L.; Cameron, R. *Proc. Inst. Mech. Eng.* **1967**, *182* (1), 307.
(69) Johnson, K. L.; Roberts, A. D. *Proc. R. Soc. London* **1974**, *A337*, 217.
(70) Johnson, K.; Tevaarwerk, J. L. *Proc. R. Soc. London* **1977**, *A336*, 215.
(71) Evans, C. R.; Johnson, K. L. *Proc. Inst. Mech. Eng.* **1986**, *200*, 303; *Proc. R. Soc. London* **1977**, *A356*, 215.
(72) Bair, S.; Winer, W. O. *Trans. ASME, J. Lubr. Technol., Ser. F* **1979**, *101*, 251; ibid. **1982**, *104*, 357.
(73) Alsaad, M.; Bair, S.; Sandborn, D. M.; Winer, W. O. *Trans. ASME, J. Lubr. Technol., Ser. F* **1978**, *100*, 404.
(74) Bair, S.; Winer, W. O. *Trans. ASME, J. Tribol.* **1990**, *112* (2), 246.
(75) Bair, S.; Winer, W. O. *Trans. ASME, J. Tribol.* **1992**, *114*, 1.
(76) Smith, F. W. *Trans. ASLE* **1962**, *5*, 142.
(77) Fein, R. S. *Trans. J. Lubr. Technol.* **1967**, *94*, 306.

Figure 12. Local stresses (in GPa), exerted by the alkane molecules on the solid gold nonuniform substrates, plotted versus x (in Å). The stresses, obtained during a sliding simulation of the near overlap system (see Figure 10a), were calculated by averaging forces across the y direction.[59] The solid and dashed lines denote the stresses on the solid top and bottom surfaces, respectively. Side views of the solid surfaces are superimposed, aiding in visualizing the relative interasperity orientation at the indicated times. Note the significant local stresses developing in front of the approaching asperities, and the asperity deformations when the stresses achieve values about 4 GPa.

junction (for example, the linear dimension of the contact zone). The coefficient $D \equiv \eta V/Gl$ is the Deborah number,[78] which is the ratio of the relaxation time of the fluid ($\tau_R = \eta/G$) to the time of passage of the fluid through a distance l in the zone $t_l = l/V$, where V is the velocity. For small values of D, associated with low viscosity fluids and low pressures, elastic effects are small and the response is dominately viscous (e.g., at small strain rates approaching the Newtonian regime, $\eta\dot\gamma = \tau$). At medium values of D (i.e., $\tau_R \geq t_l$) brought about by a highly pressure-sensitive fluid, by extreme confinement, or by high contact pressure, the fluid responds linearly and elastically (for small strain rates). Finally at high values of D, the fluid responses elastoplastically, plastically or as a vitrified fluid.[70]

In our systems the sliding of the solid surfaces induces shear flow of the lubricant which exhibits partial slip at the boundaries and establishes a velocity gradient dV_x/dz across the junction. Inspection of the molecular flow patterns revealed that in regions away from the approaching asperities the flow was laminar, Couette-like, while in the vicinity of the asperities a certain degree of vorticity developed. In general the flow may be characterized as a mixture of shear-induced and squeeze-flow modes, the latter associated with the reduction in the size of the open flow channels in the asperity regions (see Figure 10). We have also observed that as the asperities

approach each other the density and pressure of the lubricant in the interasperity zone increase, correlated with, and caused by, a slowing down of the dynamics of the confined molecules (see below).

The regime of extreme confinement of the lubricant in the interasperity zone is of particular interest in light of the aforementioned long-standing search for a proper characterization of the state of lubricants under such extreme conditions. To gain further insight into this issue we have focused on the near overlap (no) and overlapping (o) systems at the stage of small lateral distance between the asperities ($d_{aa} \approx 7$ Å corresponding to the initial stage of asperity deformation in the overlapping system, see top left configuration in Figure 10b; note that for this distance between the leading edges of the asperities the distance between the opposing inclined surfaces of the asperities is 15 Å). At this stage the localized pressure bump in front of the asperities reached values of 0.5 GPa (see Figure 12) and 2 GPa for the two systems, respectively. At this stage we stopped the sliding of the solid surfaces and allowed the systems to evolve. The dynamical relaxations of the internal pressure and density of the lubricant molecules in the interasperity zones for the two systems are displayed in Figure 13, and a measure of the segmental configurational relaxation process in the near overlap system is shown in Figure 14.

While it is likely that the relaxation process involves a spectrum of relaxation times associated with various inter- and intramolecular degrees of freedom, we may determine from Figure 13 overall relaxation times $\tau_R^{no} \approx 25$ ps and $\tau_R^o \approx 250$ ps for the two systems, respectively. Comparison of the displacement distributions for molecular segments inside and outside the interasperity zone (Figure 14),

---

(78) The Deborah number was introduced by M. Reiner (*Phys. Today* **1964** (January), 62) as the relation between the relaxation time (τ_R) and the time scale of the experiment $D = \tau_R/\tau_{exp}$. He termed his number after a passage in the victory song of the prophetess Deborah—"the mountains flow before the Lord" (Judges V, 5), which is interpreted as expressing the fact that objects which seemingly remain unchanged during the human life span, may undergo significant changes when measured on a geological time scale.
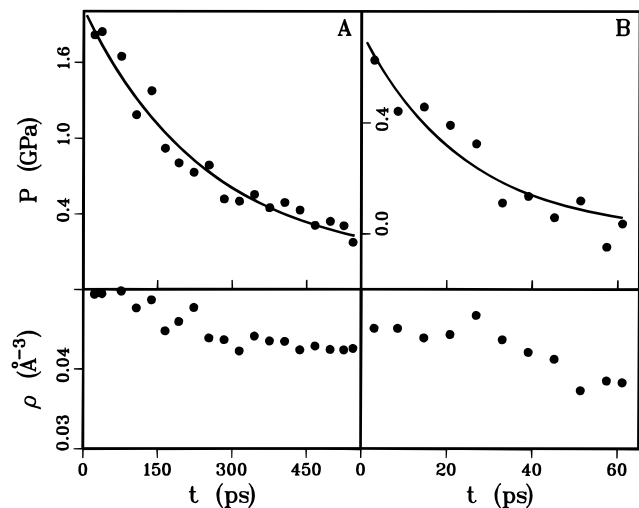
Figure 13. Plots of pressure (top) and density (bottom) versus time during the relaxation process of the elastoplastic state of the lubricant, formed under extreme confinement ($d_{aa} \sim 7$ Å), for the asperity overlap (in A) and near overlap (in B) systems. Note the difference in time scales in the two systems. The solid lines in the pressure relaxation plots correspond to least-squares fits using $P(t) = P_0 \exp(-t/\tau_R)$; $\tau_R^o = 250$ ps and $\tau_R^{no} = 25$ ps for the overlap and near overlap systems, respectively.
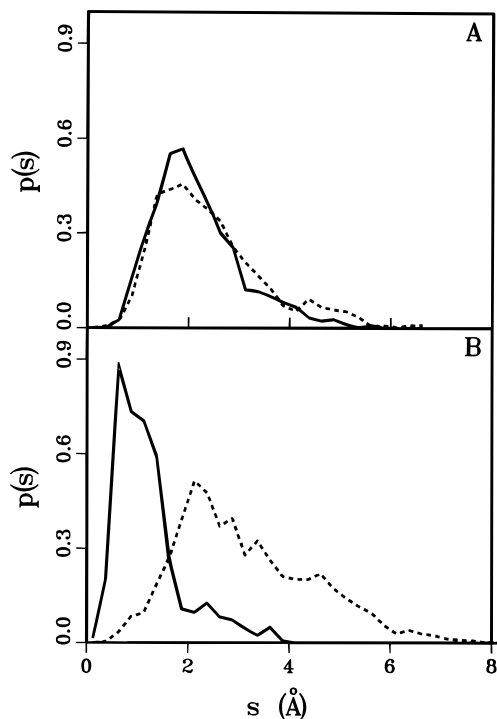

Figure 14. Distributions, $p(s)$, of a measure of the segmental displacements defined as $s = [\bar{t}^{-1} \int_0^t (\mathbf{r}_i(t) - \mathbf{r}_i(t_0))^2 \, dt]^{1/2}$, calculated for all segments, i, in a given region of the system. In our calculations we used $\bar{t} = 30$ ps. Solid (dashed) lines correspond to molecular segments inside (outside) the interasperity zone (not including boundary molecular layers, that is, only segments not bound directly to the metal are included). The distributions shown in (A) correspond to the system before sliding ($d_{aa} \sim 20$ Å), and those in (B) were calculated at the beginning of the relaxation period (see Figure 13). The significant difference between the distributions shown in (B) is a consequence of the slowed-down dynamics in the confined interasperity region.

recorded for both the equilibrium state with the two asperities at rest and well separated and during the relaxation process of the confined state, reflects the slowed-down ("sluggish") dynamics of the molecules in the densified and pressurized interasperity zone. Addition-

ally, we remark that the relaxation process involved structural rearrangements coupled to some molecular diffusion from inside the confined zone outward. For example for the overlapping system about 15% of the molecular segments left the interasperity-confined region at the end of the relaxation process ($\sim$550 ps), and the density profile along the normal to the inclined surfaces of the opposing asperities, which exhibited at the beginning of the relaxation process four squeezed layers (with the two innermost ones somewhat obliterated), relaxed at the end of the process to three well-defined sharp layers.

In light of the often conjectured characterization of the states of lubricants under extreme pressures[6,68,77] (such as "weak" elastic or plastic solids and viscoelastic or vitrified fluids), it is of interest to analyze our results in the framework of the Deborah number (see eq 2). Using the above determined relaxation times and taking for t_l the time it takes the asperities to close the gap between them (i.e., $t_l \sim 10^{-9}$ m/10 m/s $\approx$ 100 ps), we obtain $D_o \approx$ 2.5 for the overlap system and $D_{no} \approx 0.25$ for the near-overlap one. Consequently we conclude that while in the case of near overlap the lubricant response is viscoelastic with a large viscous component, the effect of enhanced confinement in the overlapping-asperity case is to create dynamically a transient medium which may be characterized as highly viscoelastic, perhaps even an elastoplastic or waxy solid. Under certain conditions the formation of such states of the lubricant may result in seizure of the contact. We remark in closing that the above observations pertain to the state and response characteristics of the lubricant in the interasperity zone. For the conditions of our simulations no shear-induced transformations were observed outside that region, nor did such transformations occur in our simulations carried out under the same conditions but with smooth Au(111) solid surfaces (i.e., with no asperities).

The dynamically varying inhomogeneity of the system causes the properties of the system (such as pressure, density, and the velocity gradient in the lubricant) to be time-dependent. Consequently, derived quantities, such as the effective viscosity, are transient and position dependent. To first approximation we calculated at various stages of the sliding process the stress in the sliding direction ($\tau_{xz} = f_x/A$, where A is the area of the solid surface), the velocity gradient in the lubricant (dV_x/dz), the effective viscosity ($\eta_{eff} = \tau_{xz}/(dV_x/dz)$), and the normal stress of the lubricant on the solid surfaces ($\tau_{zz} = f_z/A$), averaged over the whole calculational cell (see Figure 15 for the near-overlap system). These results, which were calculated up to the stage when the opposing asperities start to overlap (i.e., $d_{aa} < 0$), illustrate a significant increase in the viscosity of the system, correlated with the increased confinement and rise in pressure. They also provide an effective molecular-scale isothermal constitutive viscosity–pressure law for out system (see inset at the top of Figure 15). Similar calculations for the overlap system yielded an even sharper increase of the viscosity with $\eta_{eff} \approx 0.6$ P when $d_{aa} \sim 7$ Å. For comparison we note that for a system with smooth Au(111), surfaces sliding at the same relative velocity (10 m/s), we determined $\eta_{eff} = 0.011$ P (which is about the same as the experimental value for bulk hexadecane at 350 K). We also remark that restricting the calculations to the interasperity region results in somewhat larger viscosity and pressure values.

4. Perspectives

Understanding of tribological phenomena at the molecular scale requires the nontrivial task of unraveling the energetics, structure, dynamics, and transport processes of nonuniform systems involving a whole host of
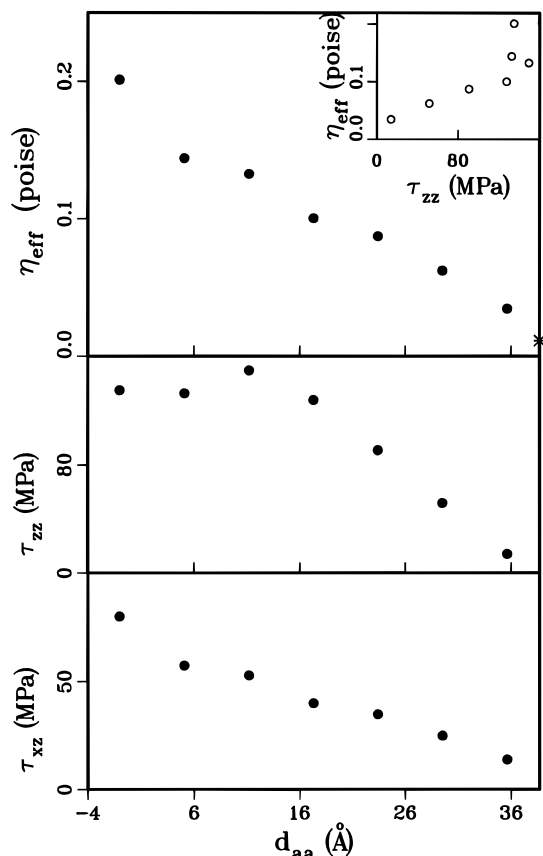
Figure 15. Variations of characteristic quantities during the sliding process of the near overlap system (see Figure 10a), plotted versus the interasperity leading-edge distance, d_{aa} (in Å). In the bottom panel we show the variations in shear stress on the solid surfaces (τ_{xz}). The velocity gradient is calculated as $dV_x/dz = V/S = 4.31$ ns^{-1}, where $V = 10$ m/s and $S = 23.2$ Å. The effective viscosity (η_{eff}) calculated from the above data is shown in the top panel exhibiting a significant increase upon confinement (smaller values of d_{aa}). The star on the right denotes $\eta_{eff} = 0.011$ P, calculated under the same conditions for a system without asperities. Also shown is the normal component of the stress (τ_{zz}), and the relationship between η_{eff} and τ_{zz}, is shown in the inset at the top.

materials (metals, ionic solids, semiconductors, ceramics, organic, and polymeric materials), under nonequilibrium conditions and often beyond the linear-response regimes for mechanical and flow behavior. Such understanding, which emerges owing to the development and proliferation of new experimental proximal probes (in particular the surface force apparatus and atomic and friction force tip-based microscopies) coupled with advances in our ability to model and simulate complex materials systems faithfully, accurately, and efficiently, is of importance from several perspectives.

First, it is often the case that understanding, initiation, and improvement of technological and engineering applications require, or are induced, by pertinent knowledge on a basic level. Understanding, on the atomic and molecular level, the origins of fundamental tribological processes (such as interfacial junction formation, nanoindentation, plastic deformations, tribochemical processes, flow, rheological states and response of confined fluid lubricants, and stick−slip phenomena) and their dependence on materials characteristics (including nature of cohesion and bonding and molecular architecture, i.e., straight chain versus branched molecular lubricants), and their dependencies on operating conditions (e.g., temperature, load, and sliding velocity), could allow ultimately

the formulation of "molecular design principles" of tribological systems.

Secondly, although our knowledge of interfacial processes occurring when two material bodies are brought together has significantly progressed since the original presentation by Heinrich Hertz before the Berlin Physical Society in January, 1881, of his theory of the contact of elastic bodies,[9] full microscopic understanding of these processes is still lacking. Moreover, it has been recognized that continuum mechanics is not fully applicable as the scale of the material bodies and the characteristic dimension of the contact between them are reduced.[79,80] Furthermore, it had long been observed[47,81] that the mechanical properties of materials exhibit a strong dependence on the size of the sample (small specimens appear to be stronger than larger ones). Since the junctions between contacting solids can be small, their mechanical properties may be drastically different from those of the same materials in their bulk form. Consequently, the application of the newly developed theoretical and experimental techniques to these problems promises to provide significant insights concerning the microscopic mechanisms and the role of surface forces in the formation of microcontacts and to enhance our understanding of fundamental issues pertaining to interfacial adherence, micro- and nanoindentation, structural deformations, and the transition from elastic to elastoplastic or fully developed plastic response of materials. Additionally, such studies allow critical assessment of the range of validity of continuum-based theories of these phenomena and could inspire improved analytical formulations.

Furthermore, theoretical investigations of tribological processes on the atomic-scale could provide the impetus for merging such refined descriptions with continuum formulations. For example, in such "hybrid" treatments, a zone comprised of a finite number of atoms (e.g., few thousand atoms), whose behavior and response can be followed with atomic-scale spatial and temporal resolution, will be embedded in a continuous medium (described, for example by means of finite element, or micro-EHL methodologies). Such formulations would allow the incorporation of atomistic response characteristics in investigations of tribological systems on spatial scales which are beyond the capability of pure atomistic treatments. Another avenue for coupling atomistic investigations with continuum-based treatments is through elucidation and determination of constitutive relationships from atomistic simulations, and their employment in continuum modeling.

Finally, atomic-scale simulations can be of great value for interpreting the results of micro- and nanotribological experiments, particularly those involving scanning-probe microscopies, the surface-force apparatus, and microbalance techniques. Moreover, understanding the behavior of materials of very small dimensions is relevant to the development of nano- and microfabricated devices and to the atomic-scale manipulation of materials. Indeed, certain current novel technologies (such as high density information storage and retrieval systems[15]), and those projected for the next century, present new tribological challenges due to the miniaturization of devices operating under extreme conditions. Elucidation of tribological processes in such devices requires atomic-scale insights, such as we have attempted to illustrate.

Our findings pertaining to molecular ordering, layering processes in lubricants confined and sheared at high

(79) Pashley, P. A. *Colloids Surf.* **1984**, *12*, 69.
(80) Pashley, M. D.; Pethica, J. B.; Tabor, D. *Wear* **1984**, *100*, 7.
(81) Gane, N. *Proc. R. Soc. London* **1970**, *A317*, 367, and references therein.

velocities by topographically nonuniform solid surfaces and their correlation with oscillatory patterns in the friction force, lubricant-mediated structural transformations and modifications of the solid surfaces, dynamical formation of elastoplastic states of the lubricant due to extreme confinement between the sliding asperities, and the appearance of post-asperity-collision nanoscale cavitated zones go beyond the predictions of continuum theories and provide the impetus for future experimental and theoretical investigations. Such investigations would include systems under various loads and different shearing velocities, lubrication under constant load conditions, thermal effects, three-dimensional asperities, multiasperity contacts, homogeneous lubricants of various chain lengths and molecular architectures, studies of lubricant mixtures, and lubricant degradation as well as tribochemical processes.